OPEN ACCESS
IOP Publishing
Journal of Physics: Condensed Matter
J. Phys.: Condens. Matter **34** (2022) 383002 (17pp)
https://doi.org/10.1088/1361-648X/ac8090

Topical Review

Solidification of ternary melts with a two-phase layer

L V Toropova[1,2,*], A A Ivanov[3], S I Osipov[4], Y Yang[5], E V Makoveeva[3] and D V Alexandrov[3]

[1] Laboratory of Mathematical Modeling of Physical and Chemical Processes in Multiphase Media, Department of Theoretical and Mathematical Physics, Ural Federal University, Ekaterinburg 620000, Russia
[2] Otto-Schott-Institut für Materialforschung, Friedrich-Schiller-Universität-Jena, Jena 07743, Germany
[3] Laboratory of Multi-Scale Mathematical Modeling, Department of Theoretical and Mathematical Physics, Ural Federal University, Ekaterinburg 620000, Russia
[4] Institute of Natural Sciences and Mathematics, Ural Federal University, Lenin Ave., 51, Ekaterinburg 620000, Russia
[5] Key Laboratory of Polar Materials and Devices and Physics Department, East China Normal University, Shanghai 200241, People's Republic of China

E-mail: l.v.toropova@urfu.ru

Received 6 May 2022, revised 4 July 2022
Accepted for publication 12 July 2022
Published 22 July 2022

Abstract

This review is concerned with the nonstationary solidification of three-component systems in the presence of two moving phase transition regions—the main (primary) and cotectic layers. A non-linear moving boundary problem has been developed and its analytical solutions have been defined. Namely, the temperature and impurity concentration distributions were determined, the solid phase fractions in the phase transition regions and the laws of motion of their boundaries were found. It was shown that variations in the initial impurity concentration affect significantly the ratio between the lengths of the two-phase layers. A non-linear liquidus surface equation is theoretically taken into account as well.

Keywords: phase transformation, mushy layer, phase diagram, ternary melt, solidification

(Some figures may appear in colour only in the online journal)

1. Introduction

The formation of crystals and complex solid phase structures from a cooled liquid or melt is a fundamental process in both industry and nature. Although some processes take place in a pure (or almost pure) liquid, most of them are the crystallization of several different components, for example, the production of various alloys and the solidification of lava [1–6]. Some of the fundamental aspects of the solidification process of multicomponent systems can be identified from the study of binary systems. In particular, studies of binary systems explain how the main substance can displace an impurity, resulting in a region of concentration supercooling. This leads to an unstable flat crystallization front [7] and the formation of a two-phase state zone of matter [8–10]. Even more complex behavior can be observed for multicomponent systems—several two-phase zones are

* Author to whom any correspondence should be addressed.

formed, each of which contains solid phases of several components.

Therefore, studies of binary systems need to generalize to more complex cases involving the consideration of a large number of significant components. Although scientists often study complex multicomponent materials, it is possible to gain an understanding of the main aspects by considering the crystallization of three major components (for example, the formation of granite from quartz, feldspar, and mica or the transport of contaminants and biological organisms in seawater [11]). In one study, Huppert and Sparks [12] proposed an explanation for the formation of oceanic basalts as a mixture of chrysolite, plagioclase, and pyroxene due to density inversion. It was important that the density of the melt first decreased due to crystallization of chrysolite, then increased again when plagioclase also underwent phase transition. In addition, the authors of [13–15] modeled three-component systems and performed calculations for nickel alloys with the presence of a two-phase zone. In [16–18] the effect of convection on the crystallization process of such alloys was shown.

Thus, the study of three-component systems generalizes the previously developed theory and provides explanations for many experimental data on the solidification of multicomponent systems. In recent laboratory experiments [19] on the crystallization of two salts dissolved in water, the present role of a small amount of one salt in the system was revealed (to eliminate convection in the system, its cooling was done from the lower boundary side). Based on experimental data presented in this work, where crystallization with two-phase transition regions (two-phase zones) was observed, a mathematical model of such processes was developed and its analytical solution was obtained.

2. Unsteady solidification of three-component systems with two-phase zones in the self-similar regime

2.1. Phase diagram and experimental data

An important part of the model and the key to understanding the solidification of three-component systems is the phase diagram (see figure 1). It shows the solid and liquid phases that can be in thermodynamic equilibrium at given component concentrations and temperatures. For three-component systems, it would be three-dimensional [20] and for real three-component systems, it can be very complicated (see [21] and [22]). In Crane's [23] model, for example, it included intermetallic phases, a peritectic point, and a cotectic point. In [24, 25] two- and three-dimensional crystallization models of three-component systems and in [26, 27] multi-component ones have been studied. We, following [19] and [28], consider a simplified model based on the assumption that each of the three components crystallizes separately and displaces all others. This case describes many water mixtures, including those studied in [19]. Such a phase diagram is shown schematically in figure 2.

Let B and C denote concentrations of substances dissolved in solvent A ($A+B+C=1$). The three angles of the phase diagram correspond to the pure substances and the vertical axis to the temperature. Each vertical plane of the phase diagram for a three-component system describes the phase diagram of a binary mixture (T_* is the phase transition temperature of the pure substance A, the eutectic point E_{AB} of the binary system has a temperature T_E^{AB} and an impurity concentration B_E^{AB}). The liquidus curves passing in each of the three vertical planes bound the three liquidus surfaces, the intersection of which forms the three cotectic curves. These curves extend from the eutectic points of binary systems (e.g. from the point E_{AB}) and intersect to give the eutectic point of the ternary system. This point corresponds to temperature T_E and concentrations of components A_E, B_E and C_E (for a more detailed discussion of phase diagrams of three-component systems see, for example, monograph [21]).

The different phases that are observed during the solidification of a three-component mixture can be defined through the solidification path on the phase diagram that the system takes. Let the three-component system be at some point P in the phase diagram. Cooling of the system leads to a phase transition of substance A from liquid to solid-state, with dissolved impurities being displaced by the growing solid phase into the liquid part of the system. This increases the concentrations of both components before the phase transition boundary and, consequently, lowers the phase transition temperature. As a result, the system undergoes a movement along the liquidus plane of the phase diagram from the point P towards some point S located on the cotectic curve. At this time, the solidifying system contains one mentioned region of phase transformation of matter A, called the main two-phase zone. When the cotectic curve reaches the point S, the phase transition begins to undergo a component B. The further path of the system in the phase diagram corresponds to its movement from point S to point E along the cotectic line, with two regions of phase transition already existing in the system—the main two-phase zone (existing on the path $P-S-E$) and the cotectic two-phase zone (existing on the path $S-E$) where substances A and B undergo the transition from the liquid state to the solid-state. When the system reaches a point E, a eutectic solid is formed consisting of components A, B, and C.

The assumption of the total immiscibility of the solid phases (see [21]) is that the solid phase of component A consists only of pure matter A. Similarly, the solid phases B and C consist of pure components B and C.

The equation of the liquidus surface passing through the point T_* of the angle BAC of the phase diagram is given as a known function of the phase transition temperature T_*^p in the main two-phase zone, which depends on the concentrations B and C:

$$T = T_*^p = F(B, C). \tag{1}$$

The cotectic line, where the section $S-E$ lies, will be set as a dependence of the phase transition temperature. In the cotectic two-phase zone, these functions are also considered to be known:

$$T = T_*^c = F_1^c(B) = F_2^c(C), \tag{2}$$

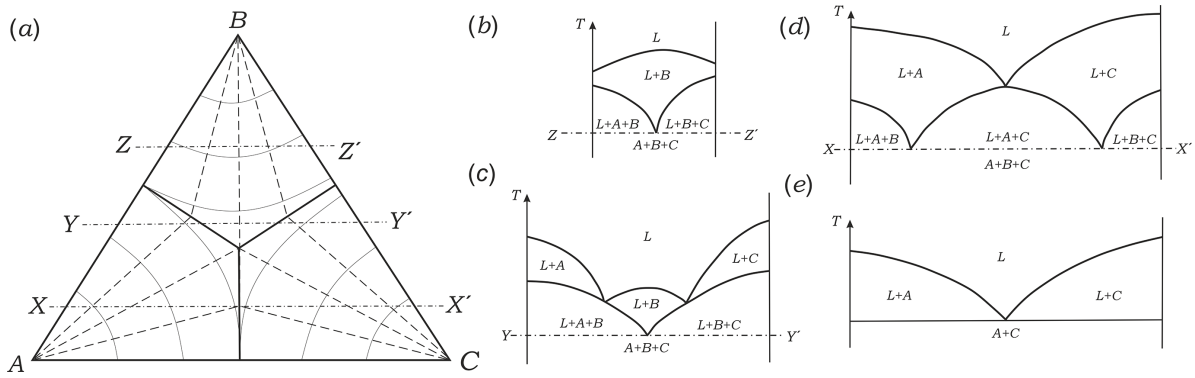

Figure 1. A view of a simple ternary phase diagram for the components A, B, C, forming pure crystals, without solid solutions. Thick lines separate the fields of the corresponding components. Thin solid lines are temperature contours on liquidus surfaces and dashed lines are temperature contours on liquidus surfaces. (a) Main view of a diagram. (b)–(d) Vertical cross-sections giving the liquid L and solids A, B, C phases present in equilibrium at a given bulk composition and temperature. (e) Binary phase diagram plotted along the AC-axis..

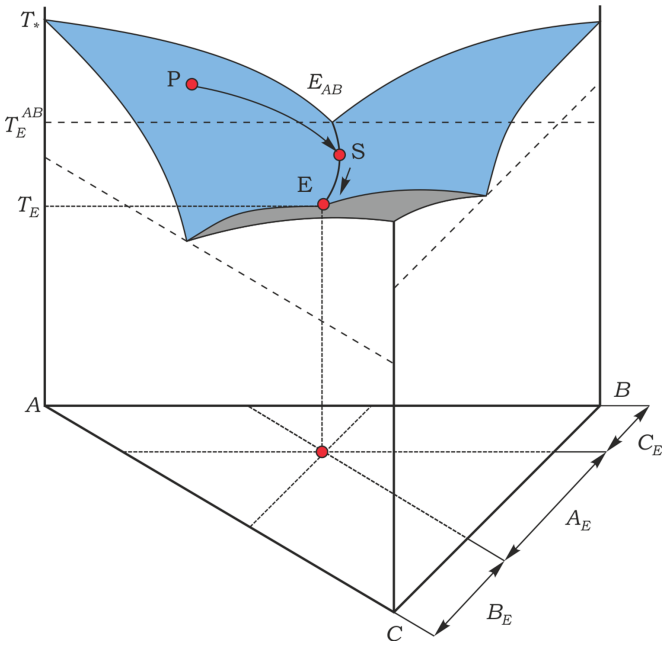

Figure 2. Phase diagram of a three-component system. Each corner of the phase diagram corresponds to pure matter A, B or C. The temperature is plotted on the vertical axis.

here it is assumed that B and C depend on coordinates and time. To determine the functions F, F_1^c and F_2^c it is necessary to know the temperature and concentration values of the components B and C at several points in the phase diagram. So, for example, in the case of linear functions (see work [28]), we arrive at:

$$T_*^p = T_* + m_B B + m_C C,$$
$$T_*^c = -m_B^c(B - B_E) + T_E = -m_C^c C + T_E^{AB}. \qquad (3)$$

To determine the slope coefficients of the liquidus lines, it is sufficient to know three points: ($B = 0$, $C = 0$, $T = T_*$—melting point), ($B = B_E^{AB}$, $C = 0$, $T = T_E^{AB}$—eutectic point of binary system), ($B = B_E$, $C = C_E$, $T = T_E$—eutectic point of three-component system). Substituting now these points into the expression (3), we find all four liquidus slope coefficients: $m_B = (T_E^{AB} - T_*)/B_E^{AB}$, $m_C = -m_C^c(1 + m_B/m_B^c)$, $m_B^c = (T_E^{AB} - T_E)/(B_E - B_E^{AB})$, $m_C^c = (T_E^{AB} - T_E)/C_E$.

Let's go into more detail about the experimental data [19]. In this work, the mixture H_2O-KNO_3-$NaNO_3$ was considered because, firstly, it is transparent and easy to observe visually; secondly, its phase diagram is simple enough, so that the experiment is close to theory; thirdly, the temperatures of the eutectics and the liquidus surfaces do not differ much from room temperature, so that no special equipment is needed; fourthly, concentrations in the liquid phase can be accurately measured. The system has a eutectic temperature of $-19.0\,^\circ$C and salt concentrations can be determined through measurement of calcium and sodium ions by spectroscopy.

Figure 3 shows the pictures of the process. In the first photo, the eutectic phase is almost invisible but the two-phase zone is visible. In the second one, the whole solid is already clearly distinguishable from the two-phase zone.

An important result of this work is the time-dependent boundary positions obtained from the experiment (figure 4) as well as the temperature distribution in the zones (figure 5). Figure 4 clearly shows that the system goes into self-similar mode after some time after the start of the process. Figure 5 introduces several conclusions: firstly, the temperature at the boundary between the main two-phase zone and the liquid remains practically constant; secondly, the temperature inside the two-phase zones and in the solid changes according to an almost linear law along the coordinate and its slope remains almost constant everywhere except the liquid phase.

2.2. *Mathematical model of the process*

Let us consider the process of directional crystallization of a three-component system from a cooled boundary $z = 0$ (see figure 6). In these processes frequently encountered in metallurgy [19, 29–31]) and geophysics [32], the boundary temperature T_B provides four regions of purely solid and liquid phases, cotectic and main two-phase zones [19]. These four regions are separated by three movable boundaries $h_p(t)$, $h_c(t)$ and $h_e(t)$ (see figure 6). Hereinafter, the indices p, c and e denote the values in the main two-phase zone, the cotectic two-phase zone and the solid phase, respectively.

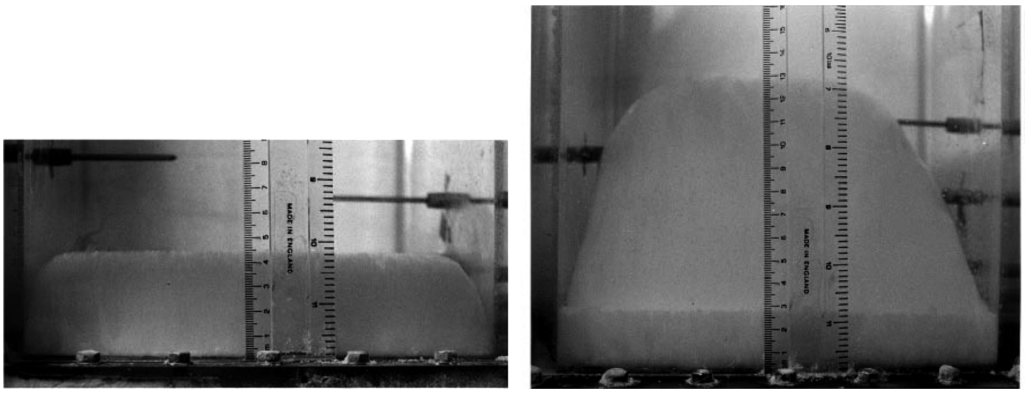

Figure 3. Photos of experiment 7 in [19]. The left photo shows the process after 5.1 h, the boundary of the two-phase zone is at 4.7 cm, the eutectic zone is 0.3 cm and almost invisible. On the right, after 82.5 h, the eutectic front has grown to 2.7 cm, the two-phase zone to 14.4 cm.

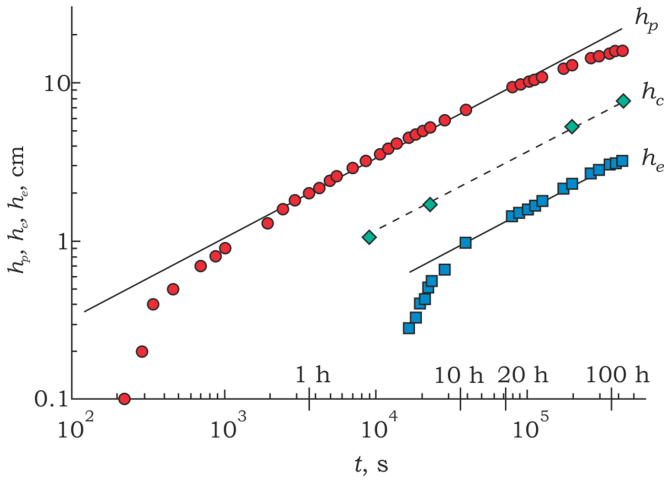

Figure 4. Boundary positions according to experiment 7 in [19] in logarithmic coordinates. Here h, h_C and h_E are boundary positions between liquid phase and main two-phase zone, main and cotectic zone, cotectic two-phase zone and solid phase, respectively.

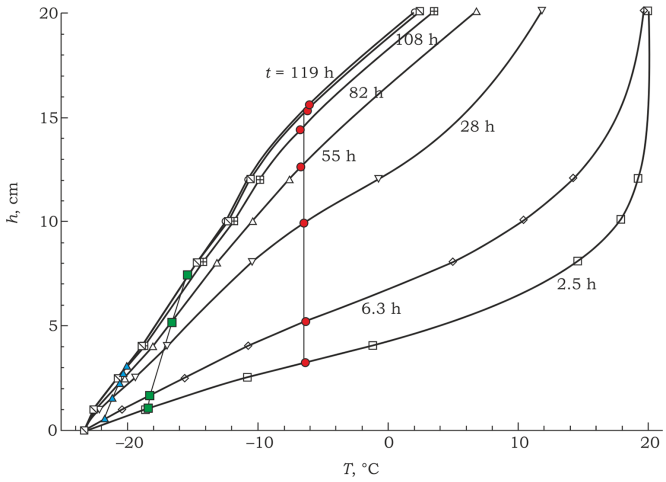

Figure 5. Temperature distribution according to experiment 7 in [19] for different time points (numbers at the curves). The red circles indicate the position of the boundary between the liquid phase and the main two-phase zone, the green squares indicate the phase interface between the main and cotectic zones, the blue triangles illustrate the boundary between the cotectic and eutectic zones.

The heat and mass transfer equations and boundary conditions can be derived from the same assumptions as in the binary two-phase model [33]. The unknown parameters are temperature T, concentrations of components A, B and C, fractions of solid phases φ_A, φ_B and φ_C, fraction of liquid phase χ and boundary positions h_p, h_c and h_e. It is assumed that there are no flows in the liquid and the impurity distribution coefficient corresponds to the formation of pure solid component phases [23].

Boundary conditions far from the crystallization front can be written as:

$$B = B_\infty, \quad C = C_\infty, \quad T = T_\infty, \quad z \to \infty. \tag{4}$$

Equations of heat and mass transfer in a liquid are:

$$\frac{\partial B_\ell}{\partial t} = D_B \frac{\partial^2 B_\ell}{\partial t^2}, \quad \frac{\partial C_\ell}{\partial t} = D_C \frac{\partial^2 C_\ell}{\partial t^2}, \quad z > h_p(t), \tag{5}$$

$$\frac{\partial T_\ell}{\partial t} = \kappa_\ell \frac{\partial^2 T_\ell}{\partial t^2}, \quad z > h_p(t), \tag{6}$$

$$\chi = 1 \quad (\varphi_A = \varphi_B = \varphi_C = 0), \quad z > h_p(t), \tag{7}$$

where D_i is the diffusion coefficient of component i ($i = B$ or $i = C$), κ_ℓ is the thermal diffusivity coefficient of the fluid. In these equations, we neglect thermodiffusion effect [34, 35] due to its insignificant contribution.

Boundary conditions at the phase interface between the main two-phase zone and the liquid can be written as:

$$\rho_s L \varphi_{AP}^- \frac{dh_p}{dt} = k_m \left(\frac{\partial T_p}{\partial z}\right)\Big|_{h_p^-} - k_\ell \left(\frac{\partial T_\ell}{\partial z}\right)\Big|_{h_p^+}, \quad z = h_p(t), \tag{8}$$

$$B_{pb} \varphi_{AP}^- \frac{dh_p}{dt} = D_B \chi_P^- \left(\frac{\partial B_p}{\partial z}\right)|_{h_p^-} - D_B \left(\frac{\partial B_\ell}{\partial z}\right)|_{h_p^+}, \quad z = h_p(t), \tag{9}$$

$$C_{pb} \varphi_{AP}^- \frac{dh_p}{dt} = D_C \chi_P^- \left(\frac{\partial C_p}{\partial z}\right)|_{h_p^-} - D_C \left(\frac{\partial C_\ell}{\partial z}\right)|_{h_p^+}, \quad z = h_p(t), \tag{10}$$

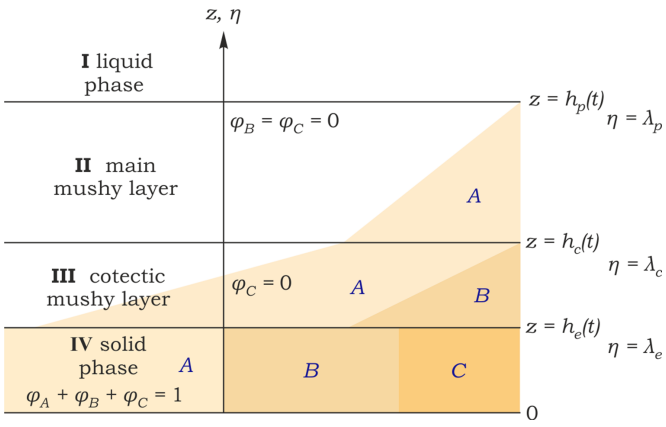

Figure 6. Schematic diagram of the solidification process of a three-component system along the spatial axis z; h_p, h_c and h_e show the positions of the phase transition boundaries as functions of time t. The shaded areas denote the amount of solid phase components A, B and C (B and C are dissolved in solvent A, $A+B+C=1$).

$$T_\ell = T_p = T_{pb} = T_*^p = F(B_{pb}, C_{pb}),$$
$$B_\ell = B_p = B_{pb}, \quad C_\ell = C_p = C_{pb}, \quad z = h_p(t), \tag{11}$$

$$\left.\frac{\partial T_\ell}{\partial z}\right|_{h_p^+} = \left.\frac{\partial F}{\partial z}\right|_{h_p^+}, \quad z = h_p(t), \tag{12}$$

here φ_{AP}^- and χ_P^- are the values of solid phase fraction of the component A and liquid phase on the left side of the boundary, T_{pb}, B_{pb} and C_{pb} are values of temperature and component concentrations at the boundary $z = h_p(t)$, respectively. The expression (11) includes the local thermodynamic equilibrium condition meaning that the temperature at the boundary is equal to the phase transition temperature of the liquidus surface. The last relation (12) represents a limit equilibrium condition at the boundary.

Let's assume that thermal properties of all solid phases are the same, but different from liquid phase properties. Thermophysical properties in two-phase zones can be written as:

$$k_m = k_\ell\chi + k_A\varphi_A + k_B\varphi_B + k_C\varphi_C = k_\ell\chi + k_s(1-\chi), \tag{13}$$

$$\rho_m c_m = \rho_\ell c_\ell \chi + \rho_s c_s (1-\chi). \tag{14}$$

In addition, we take one value for the latent heat of solidification for all components ($L = L_A = L_B = L_C$).

The heat and mass transfer equations in the main (primary) two-phase zone can be written as:

$$\rho_m c_m \frac{\partial T_p}{\partial t} = \frac{\partial}{\partial z}\left(k_m \frac{\partial T_p}{\partial z}\right) + L\frac{\partial \varphi_A}{\partial t}, \quad h_c(t) < z < h_p(t), \tag{15}$$

$$\chi\frac{\partial B_p}{\partial t} = D_B\frac{\partial}{\partial z}\left(\chi\frac{\partial B_p}{\partial z}\right) + B_p\frac{\partial \varphi_A}{\partial t}, \quad h_c(t) < z < h_p(t), \tag{16}$$

$$\chi\frac{\partial C_p}{\partial t} = D_C\frac{\partial}{\partial z}\left(\chi\frac{\partial C_p}{\partial z}\right) + C_p\frac{\partial \varphi_A}{\partial t}, \quad h_c(t) < z < h_p(t), \tag{17}$$

$$T_p = T_*^p = F(B_p, C_p), \quad h_c(t) < z < h_p(t), \tag{18}$$

$$\chi + \varphi_A = 1 \ \ (\varphi_B = \varphi_C = 0), \quad h_c(t) < z < h_p(t). \tag{19}$$

Boundary conditions between two mushy zones take the form:

$$\rho_s L(-\chi_C^- + \chi_C^+)\frac{dh_c}{dt} = k_m(\chi_C^-)\left(\frac{\partial T_c}{\partial z}\right)|_{h_c^-} - k_m(\chi_C^+)\left(\frac{\partial T_p}{\partial z}\right)|_{h_c^+}, \quad z = h_c(t), \tag{20}$$

$$\left[-B_{cb}(\chi_C^- - \chi_C^+) + -\varphi_{BC}^-\right]\frac{dh_c}{dt} = D_B\chi_C^-\left(\frac{\partial B_c}{\partial z}\right)\Big|_{h_c^-} - D_B\chi_C^+\left(\frac{\partial B_p}{\partial z}\right)\Big|_{h_c^+}, \quad z = h_c(t), \tag{21}$$

$$C_{cb}(-\chi_C^- + \chi_C^+)\frac{dh_c}{dt} = D_C\chi_C^-\left(\frac{\partial C_c}{\partial z}\right)\Big|_{h_c^-} - D_C\chi_C^+\left(\frac{\partial C_p}{\partial z}\right)\Big|_{h_c^+}, \quad z = h_c(t), \tag{22}$$

$$T_p = T_c = T_{cb} = F(B_{cb}, C_{cb}) = F_1^c(B_{cb}) = F_2^c(C_{cb}), \quad z = h_c(t), \tag{23}$$

$$C_p = C_c = C_{cb}, \quad B_p = B_c = B_{cb}, \quad z = h_c(t), \tag{24}$$

$$\left.\frac{\partial F_1^c}{\partial z}\right|_{h_c^+} = \left.\frac{\partial F_2^c}{\partial z}\right|_{h_c^+}, \quad z = h_c(t), \tag{25}$$

here χ_C and φ_{BC} are the values of phase fractions at the interface, the symbols '+' and '−' denote the side of the interface at which the value is taken, T_{cb}, B_{cb} and C_{cb} are the temperature and component concentrations at the interface $z = h_c(t)$.

The relation (25) is the limiting equilibrium condition for the interface between two two-phase zones. Mathematically, it means that the crystallization at the liquidus surface moves to the cotectic line smoothly [28] and tangentially. Physically, this condition shows that there is no oversaturation of the second solidification component B at the boundary.

In the cotectic two-phase zone, the heat-mass transfer equations are:

$$\rho_m c_m \frac{\partial T_c}{\partial t} = \frac{\partial}{\partial z}\left(k_m\frac{\partial T_c}{\partial z}\right) + L\frac{\partial(\varphi_A + \varphi_B)}{\partial t}, \quad h_e(t) < z < h_c(t), \tag{26}$$

$$\chi\frac{\partial B_c}{\partial t}=D_B\frac{\partial}{\partial z}\left(\chi\frac{\partial B_c}{\partial z}\right)+B_c\frac{\partial(\varphi_A+\varphi_B)}{\partial t}-\frac{\partial\varphi_B}{\partial t},\quad h_e(t)<z<h_c(t),\tag{27}$$

$$\chi\frac{\partial C_c}{\partial t}=D_C\frac{\partial}{\partial z}\left(\chi\frac{\partial C_c}{\partial z}\right)+C_c\frac{\partial(\varphi_A+\varphi_B)}{\partial t},\quad h_e(t)<z<h_c(t),\tag{28}$$

$$T_c=T_*^c=F_1^c(B_c)=F_2^c(C_c),\quad h_e(t)<z<h_c(t),\tag{29}$$

$$\chi+\varphi_A+\varphi_B=1\ \ (\varphi_C=0),\quad h_e(t)<z<h_c(t).\tag{30}$$

Note that the formation of the solid phase of component B leads to a decrease in the concentration of this component in the liquid. Ratio (29) shows that crystallization proceeds along the cotectic line.

Heat and mass conditions at the solid phase boundary read as:

$$\rho_s L\chi_E^+\frac{dh_e}{dt}=k_s\left(\frac{\partial T_s}{\partial z}\right)|_{h_e^-}-k_m(\chi_E^+)\left(\frac{\partial T_c}{\partial z}\right)|_{h_e^+},\quad z=h_e(t),\tag{31}$$

$$c\left[B_s-\varphi_{BE}^--B_c(1-\chi_E^+)+\varphi_{BE}^+\right]\frac{dh_e}{dt}=-D_B\chi_E^+\left(\frac{\partial B_c}{\partial z}\right)|_{h_e^+},\quad z=h_e(t),\tag{32}$$

$$\left[C_s-\varphi_{CE}^--C_c(1-\chi_E^+)\right]\frac{dh_e}{dt}=-D_C\chi_E^+\left(\frac{\partial C_c}{\partial z}\right)|_{h_e^+},\quad z=h_e(t),\tag{33}$$

$$T_c=T_s=F_1^c(B_E)=F_2^c(C_E)=T_E,\quad z=h_e(t),\tag{34}$$

$$C_c=C_s=C_E,\quad B_c=B_s=B_E,\quad z=h_c(t).\tag{35}$$

Here χ_E^+ and φ_{BE}^+ are values of phase fractions to the right of the boundary, φ_{BE}^- and φ_{CE}^- are to the left of the boundary, T_E, B_E and C_E are temperature and concentration values of components at the boundary $z=h_e(t)$, correspond to the eutectic point of the three-component system, respectively.

The heat condition equation in a solid can be written as:

$$\frac{\partial T_s}{\partial z}=\kappa_s\frac{\partial^2 T_s}{\partial z^2},\quad 0<z<h_e(t).\tag{36}$$

Apart from that, we have the following:

$$\varphi_A+\varphi_B+\varphi_C=1\ \ (\chi=0),\quad 0<z<h_e(t),\tag{37}$$

and *at the cooled boundary*:

$$T_s=T_B<T_E,\quad z=0.\tag{38}$$

Diffusion in the solid phase is neglected.

2.3. Linear temperature profile and integration of diffusion equations in two-phase zones

According to the experimental data, the temperature field in the two-phase zones and solid phase is practically a linear function of the spatial coordinate z (that is shown in figure 5). This occurs quite frequently in problems of this type (see, for example, [36–39]) and can be explained by the fact that the relaxation time of the temperature field is a few orders of magnitude smaller than the relaxation time of the diffusion fields and the interphase boundary motion. Therefore, the temperature field in the main two-phase zone at $h_c(t)<z<h_p(t)$ will be considered as a linear function:

$$T_p(z,t)=T_1(t)+T_2(t)z,\tag{39}$$

where T_1 and T_2 are time dependent functions defined by the solution.

Using this dependence it is possible to integrate the diffusion equations in the main two-phase zone (16) and (17) in a general form. Neglecting the first term in equation (15) due to very fast relaxation of the temperature field and using expression (39), from (15) we obtain:

$$T_2(t)\frac{\partial\varphi_A}{\partial z}=-\frac{L}{k_s-k_l}\frac{\partial\varphi_A}{\partial t}.\tag{40}$$

Substituting (39) and (40) into (16) and (17), we arrive at the expressions for the component concentration fields as:

$$B_p(z,t)=\frac{B_{pb}+b_2T_D\varphi_A}{1-\varphi_A},\quad C_p(z,t)=\frac{C_{pb}+c_2T_D\varphi_A}{1-\varphi_A},\quad T_D=\frac{D_BL}{k_s-k_l},\tag{41}$$

where we assumed the case $D_B=D_C$ (B_{pb} and C_{pb} are concentration values at the boundary $z=h_p$ and $\varphi_A=0$, respectively). In addition, we suppose that the concentrations of the components B and C are linear along the spatial coordinate z with gradients $B_2(t)=b_2\,T_2(t)$ and $C_2(t)=c_2T_2(t)$ proportional to the temperature gradient, i.e. $B_p(z,t)=B_1(t)+B_2(t)z$ and $C_p(z,t)=C_1(t)+C_2(t)z$ (B_1 and C_1 are linear terms in the z expansion).

Taking (39) into account, let us substitute the concentration fields (41) into (3), and obtain an expression for the solid phase fraction in the main two-phase zone in a form:

$$\varphi_A(z,t)=\frac{T_1+zT_2-T_*-m_BB_{pb}-m_CC_{pb}}{T_1+zT_2-T_*+T_D},\tag{42}$$

where the expression $m_Bb_2+m_Cc_2=1$ follows from (41) with account of equation (39). Combining (41) and (42), we can find b_2 and c_2 as:

$$b_2=\frac{B_{pb}}{m_BB_{pb}+m_CC_{pb}},\quad c_2=\frac{C_{pb}}{m_BB_{pb}+m_CC_{pb}}.$$

Substituting these values and (42) into (41) we arrive at the final expressions for the concentrations of the components in the main (primary) two-phase zone:

$$B_p(z,t) = \frac{B_{pb}(T_1 - T_* + zT_2)}{m_B B_{pb} + m_C C_{pb}}, \quad C_p(z,t) = \frac{C_{pb}(T_1 - T_* + zT_2)}{m_B B_{pb} + m_C C_{pb}}. \tag{43}$$

Due to the fact that the impurity diffusion in the liquid phase at $z \geqslant h_p(t)$ directly follows the boundary displacement h_p (see [19]), we will take the following boundary conditions for the concentration at $z = h_p(t)$ instead of (9) and (10):

$$(B_{pb} - B_\infty)\frac{dh_p}{dt} = -D_B\frac{\partial B_p}{\partial z}, \quad (C_{pb} - C_\infty)\frac{dh_p}{dt} = -D_C\frac{\partial C_p}{\partial z}, \tag{44}$$

where B_∞ and C_∞ are the values of impurity concentrations in the liquid far away from the boundary $z = h_p(t)$.

Substituting the distribution (43) into the boundary conditions (44) we obtain ($D_B = D_C$):

$$C_{pb} = \frac{C_\infty}{B_\infty}B_{pb}. \tag{45}$$

Combining (45) with the first equations in (43) and (44), we have:

$$(B_{pb} - B_\infty)(m_B B_\infty + m_C C_\infty)\frac{dh_p}{dt} = -D_B B_\infty T_2. \tag{46}$$

Equating (3) to the boundary temperature T_{pb} at $z = h_p$ and using (45), we express the boundary concentration value of component B:

$$B_{pb} = \frac{(T_{pb} - T_*)B_\infty}{m_B B_\infty + m_C C_\infty}. \tag{47}$$

Substituting B_{pb} from the last expression into (46), and the distribution (39) into the boundary point $z = h_p$, we find the time dependences of the temperature field in the main two-phase zone as:

$$T_1(t) = T_{pb} - h_p(t)T_2(t),$$

$$T_2(t) = \frac{1}{D_B}\left(m_B B_\infty + m_C C_\infty + T_* - T_{pb}\right)\frac{dh_p}{dt}.$$

Due to the practically constant temperature boundary value T_{pb} (see [19] and figure 5), the solution of the heat conduction equation at $z > h_p(t)$ can be represented as:

$$T_\ell(z,t) = T_\infty + (T_{pb} - T_\infty)\frac{\operatorname{erfc}(z/2\sqrt{\kappa_\ell t})}{\operatorname{erfc}(h_p(t)/2\sqrt{\kappa_\ell t})}, \tag{48}$$

where T_∞ is the temperature in the unperturbed part of the fluid and κ_ℓ is its thermal diffusivity coefficient. Note specifically that the solution (48) is valid only for a constant temperature T_{pb} or for weak temporal oscillations.

Taking the equality of heat fluxes at $z = h_p(t)$ ($\varphi_A = 0$), $\partial T_\ell/\partial z = \partial T_p/\partial z$, from (39) and (47) we obtain an equation that links two unknown parameters such as the boundary position $h_p(t)$ and the temperature T_{pb}:

$$\frac{(T_\infty - T_{pb})D_B}{\sqrt{\pi\kappa_\ell t}(m_B B_\infty + m_C C_\infty + T_* - T_{pb})} = \operatorname{erfc}\left(\frac{h_p(t)}{2\sqrt{\kappa_\ell t}}\right)\exp\left(\frac{h_p^2}{4\kappa_\ell t}\right)\frac{dh_p}{dt}. \tag{49}$$

Because the relaxation time of the temperature field in the cotectic two-phase zone is much shorter than the relaxation time of the diffusion fields, we consider the temperature in the zone as linear in spatial coordinate (see figure 5):

$$T_c(z,t) = T_3(t) + zT_4(t). \tag{50}$$

Mathematically, this expression for temperature approximately satisfies the heat transfer equation (26). In addition, the component concentrations and temperature in the cotectic two-phase zone are related by the equation (3). Taking (50) into account, we obtain:

$$B_c(z,t) = -\frac{1}{m_B^c}(T_3 + zT_4 - T_E) + B_E,$$
$$C_c(z,t) = -\frac{1}{m_C^c}(T_3 + zT_4 - T_E^{AB}). \tag{51}$$

As previously, we omit the left-hand side of equation (15) and consider the linearity of the temperature profile. This yields a relationship similar to (40) as:

$$T_4\frac{\partial(1 - \varphi_A - \varphi_B)}{\partial z} = -\frac{L}{k_s - k_\ell}\frac{\partial(1 - \varphi_A - \varphi_B)}{\partial t}. \tag{52}$$

Now, combining (27), (28), (51) and (52), we obtain the following concentration distributions in the cotectic two-phase zone:

$$B_c(z,t) = \frac{T_D(\chi - \chi_C^-)/m_B^c + B_{cb}\chi_C^- + \varphi_{BC}^- - \varphi_B}{\chi}, \tag{53}$$

$$C_c(z,t) = \frac{T_D(\chi - \chi_C^-)/m_C^c + C_{cb}\chi_C^-}{\chi}, \tag{54}$$

where $\chi_C^- = 1 - \varphi_{AC}^- - \varphi_{BC}^-$, $\chi(z,t) = 1 - \varphi_A(z,t) - \varphi_B(z,t)$, B_{cb} and C_{cb} are concentration values at $z = h_c(t)$, φ_{AC}^- and φ_{BC}^- mean φ_A and φ_B, respectively, to the left of the boundary $z = h_c(t)$.

Experimental data show that the temperature field in the solid phase and both two-phase zones are almost the identical linear function. Thus, we consider the case where $T_1 = T_3$ and $T_2 = T_4$.

By equating the distributions (43) and (53) or (54) at $z = h_c(t)$ (either of these can be used) with the expression for T_1, we can find the interface coordinate of the two phase zones as:

$$h_c(t) = h_p(t) + \frac{m_C^c C_\infty T_* + T_E^{AB}R - T_{pb}(m_C^c C_\infty + R)}{(m_C^c C_\infty + R)T_2}, \tag{55}$$

where $R = m_B B_\infty + m_C C_\infty$.

Substituting h_c from (55) into (42) at $z = h_c$, we obtain the solid phase fraction to the right of the interface:

$$\varphi^+_{AC} = 1 - \frac{(B_{pb}R + T_D B_\infty)(m^c_C C_\infty + R)}{B_\infty[(T^{AB}_E - T_* + T_D)R + T_D m^c_C C_\infty]}. \quad (56)$$

The fractions distributions χ of liquid phase, φ_A and φ_B of solid phase in the cotectic zone are determined by equations (51), (53) and (54). By equating the left-hand sides of these expressions, we arrive at:

$$\varphi_B(z,t) = \varphi^-_{BC} + \left(B_{cb} - \frac{T_D}{m^c_B}\right)\chi^-_C + \frac{(T_1 + zT_2 - T_E - m^c_B B_E + T_D)(T_D - m^c_C C_{cb})}{m^c_B(T_1 + zT_2 - T^{AB}_E + T_D)}\chi^-_C, \quad (57)$$

$$\varphi_A(z,t) = 1 - \varphi_B(z,t) - \frac{(T_D - m^c_C C_{cb})\chi^-_C}{T_1 + zT_2 - T^{AB}_E + T_D}. \quad (58)$$

The boundary values φ^-_{AC} and φ^-_{BC} to the left of the boundary $z = h_c(t)$ are found explicitly from the boundary conditions (21) and (22) of the mass balance at $z = h_c(t)$. Assuming the distributions (43) and (51), $D_B = D_C$ and $T_2 = T_4$, we rewrite these equations as:

$$m^c_B R\left(B_{cb}(\varphi^+_{AC} - \varphi^-_{AC} - \varphi^-_{BC}) + \varphi^-_{BC}\right)\frac{dh_c}{dt} = D_B T_2\left((1 - \varphi^+_{AC})m^c_B B_\infty + (1 - \varphi^-_{AC} - \varphi^-_{BC})R\right), \quad (59)$$

$$m^c_C R C_{cb}(\varphi^+_{AC} - \varphi^-_{AC} - \varphi^-_{BC})\frac{dh_c}{dt} = D_B T_2\left((1 - \varphi^+_{AC})m^c_C C_\infty + (1 - \varphi^-_{AC} - \varphi^-_{BC})R\right). \quad (60)$$

Finally, we obtain:

$$\chi^-_C = \frac{m^c_C \chi^+_C\left(RC_{cb}\frac{dh_c}{dt} + D_B T_2\, C_\infty\right)}{R(m^c_C C_{cb}\frac{dh_c}{dt} - D_B T_2)}, \quad (61)$$

$$\varphi^-_{BC} = \frac{D_B T_2(\chi^+_C m^c_B B_\infty + \chi^-_C R)}{m^c_B R\frac{dh_c}{dt}} - \frac{m^c_B R\frac{dh_c}{dt}B_{cb}(\chi^-_C - \chi^+_C)}{m^c_B R\frac{dh_c}{dt}}, \quad (62)$$

$$\varphi^-_{AC} = 1 - \varphi^-_{BC} - \chi^-_C. \quad (63)$$

We especially note that from the continuity of concentrations at $z = h_c$ follows $B_{cb}C_\infty = C_{cb}B_\infty$ (according to expressions (43)).

The temperature distribution $T_s(z,t)$ in the solid phase (at $0 < z < h_e(t)$) is linear and almost coincides with the temperature profile in both two-phase zones. Therefore, we have:

$$T_s(z,t) = T_B + \frac{T_E - T_B}{h_e(t)}z, \quad T_1(t) + h_e(t)T_2(t) = T_E,$$

whence it follows that:

$$h_e(t) = \frac{T_E - T_1}{T_2} = h_p(t) + \frac{T_E - T_{pb}}{T_2}. \quad (64)$$

Due to the same temperature slope $T_E - T_B = T_2\ h_e$, we define the boundary solid phase—cotectic zone as:

$$h_e(t) = \frac{T_E - T_B}{T_{pb} - T_B}h_p(t). \quad (65)$$

Eliminating h_e from expressions (64) and (65), we find the law of motion of the two-phase zone-liquid boundary (at a constant value of T_{pb}):

$$h_p(t) = \sqrt{\alpha D_B t + h_p(0)}, \quad \alpha = \frac{2(T_{pb} - T_B)}{R + T_* - T_{pb}}. \quad (66)$$

Substituting h_p from (66) into (49), we obtain the temperature T_{pb} ($h_p(0) = 0$):

$$\frac{T_\infty - T_{pb}}{T_{pb} - T_B}\sqrt{\frac{\alpha D_B}{\pi\kappa_\ell}} = \operatorname{erfc}\left(\sqrt{\frac{\alpha D_B}{4\kappa_\ell}}\right)\exp\left(\frac{\alpha D_B}{4\kappa_\ell}\right).$$

Specifically, it follows from the expressions (55), (65) and (66) that all boundaries move in proportion to the square root of time.

Considering that $T_{pb} - T_B = T_2\ h_p$ and $dh_p/dt = \alpha D_B/(2h_p)$, we rewrite the boundary velocity between zones as:

$$\frac{dh_c}{dt} = \frac{D_B}{h_p}P, \quad P = \frac{m^c_C C_\infty(T_* - T_B) + R(T^{AB}_E - T_B)}{(R + T_* - T_{pb})(m^c_C C_\infty + R)}. \quad (67)$$

Further, we can find the exact expressions for the solid phase fractions φ^-_{AC} and φ^-_{BC} in the form:

$$\varphi^-_{BC} = C_{cb}(\varphi^+_{AC} - x)\frac{B_\infty(1 - \varphi^+_{AC}) + (1 - x)R/m^c_B}{C_\infty(1 - \varphi^+_{AC}) + (1 - x)R/m^c_C} + B_{cb}(x - \varphi^+_{AC}),$$

$$\varphi^-_{AC} = x - \varphi^-_{BC},$$

$$x = \frac{C_\infty(T_{pb} - T_B)(1 - \varphi^+_{AC}) + R(T_{pb} - T_B)/m^c_C - PRC_{cb}\varphi^+_{AC}}{(T_{pb} - T_B)R/m^c_C - PRC_{cb}}.$$

The boundary values of φ^+_{AE} and φ^+_{BE} (of the solid phase fraction to the right of the solid phase—cotectic zone boundary) are easily found by substituting $z = h_e(t)$ into the distributions (57) and (58). The values of φ^-_{AE}, φ^-_{BE} and φ^-_{CE} left of the boundary can be obtained from the mass balance condition (32) and (33) at $z = h_e(t)$:

$$\varphi^-_{BE} = -\frac{D_B\chi^+_E T_2}{m^c_B dh_e/dt} + B_E\chi^+_E + \varphi^+_{BE}, \quad \chi^+_E = 1 - \varphi^+_{AE} - \varphi^+_{BE},$$

$$\varphi^-_{CE} = -\frac{D_C\chi^+_E T_2}{m^c_C dh_e/dt} + C_E\chi^+_E, \quad \varphi^-_{AE} = 1 - \varphi^-_{BE} - \varphi^-_{CE}.$$

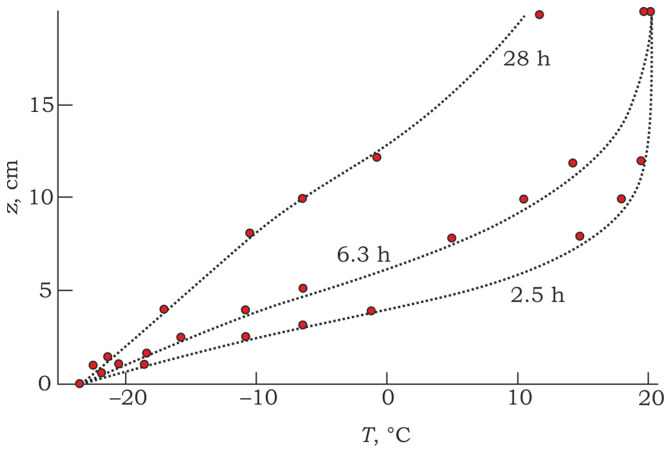

Figure 7. Temperature distribution according to the developed theory and the experimental data (black circles) of [19] (experiment 7) at different points in time (numbers at the curves). The system parameter values are taken from [19, 28].

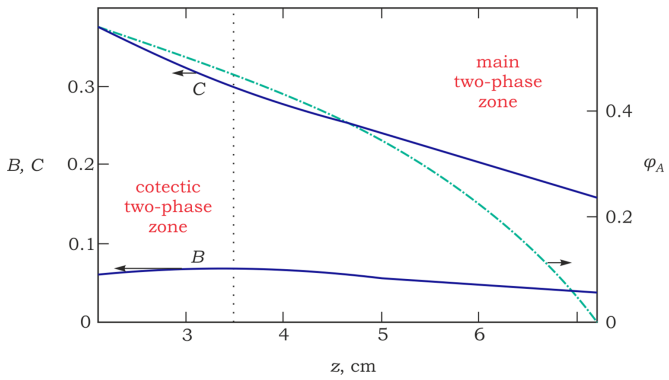

Figure 8. Impurity concentrations of components B and C (B corresponds to KNO_3, C to $NaNO_3$) and solid phase fraction of component A in two-phase state zones as a function of spatial coordinate. The vertical line shows the position of the interface between the two-phase zones.

Thus, the problem of directional solidification of a three-component system can be solved analytically using small, physically explainable and experimentally consistent assumptions.

Figures 7 and 8 show distributions of temperature, component concentrations and solid phase fraction for the system H_2O-KNO_3-$NaNO_3$ with thermophysical parameters given in table 1. The temperature field inside the solid phase and the two-phase zones, due to its fast relaxation, is well described by linear dependences, deviation from which is observed in the liquid phase due to the movement of interphase boundaries and the constancy of the temperature T_∞ maintained in the liquid. As expected, the solid phase fractions decrease with increasing spatial coordinate in both two-phase zones, cotectic and main, in agreement with the heat and mass transfer equations. The concentration of component C decreases with increasing spatial coordinate due to displacement of impurity by growing solid phase. Its change is shown in figure 9. In contrast, the concentration of component B has a weakly pronounced maximum (see figure 10), which is located at the interface of

Table 1. Thermophysical properties and control parameters of the system H_2O(A)-KNO_3(B)-$NaNO_3$(C) (from experiment 7 in [19]).

Parameter	Value
Impurity distribution coefficient (k)	2.8×10^{-10}
Melting temperature of component A (T_*, ° C)	0
Temperature of the cooled boundary (T_B, ° C)	−23.3
Temperature at the eutectic point of a three component system (T_E, ° C)	−19
Temperature at the eutectic point of a binary system $A-B$ (T_E^{AB}, ° C)	−5
Concentration of component B at the eutectic point of a three-component system (B_E, at%)	0.06
Concentration of component C at the eutectic point of a three component system (C_E, at%)	0.37
Concentration of component B at the eutectic point of a binary system $A-B$ (B_E^{AB}, at%)	0.1
Initial liquid temperature (T_∞, ° C)	20
Initial concentration of component B (B_∞, at%)	0.035
Initial concentration of component C (C_∞, at%)	0.152

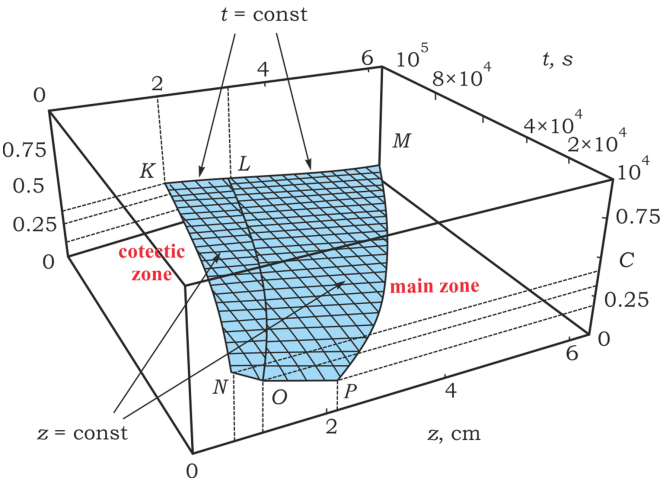

Figure 9. The concentration of component C (corresponding to $NaNO_3$) as a function of spatial coordinate z and time t. The points N, O, P and K, L, M lie on planes $t = 10^4$ and $t = 10^5$ s, respectively. The values of the parameters of the system are taken from [19, 28].

the two-phase zones (this behavior has been previously documented experimentally [19]). This function is increasing in the cotectic zone and decreasing in the main zone (distributions (43) and (51); [28] shows that m_B, m_C and m_B^c are negative). This behavior is explained by the fact that in the two-phase cotectic zone the component B undergoes a phase transition into a solid state, which leads to a decrease in its concentration as it approaches the h_e front.

3. Non-linearities in phase diagram curves and temperature during the solidification of three-component systems with two-phase zones

The method derived in the previous section for solving the problem of directional solidification of three-component systems with two-phase zones includes the assumption of linearity of the liquidus surface and temperatures in the zones.

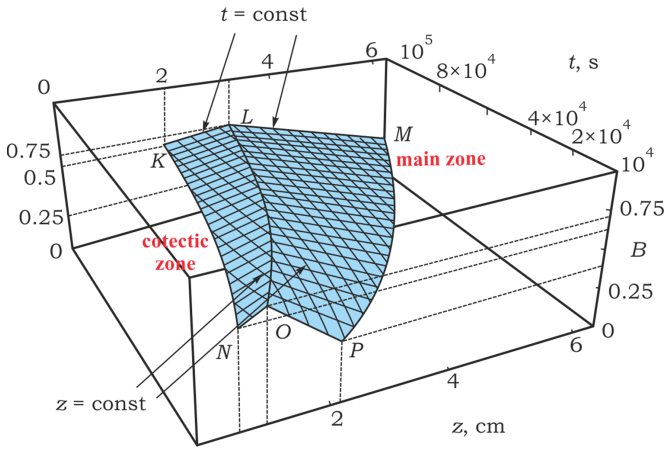

Figure 10. The concentration of component B (corresponding to KNO_3) as a function of spatial coordinate z and time t. The points N, O, P and K, L, M lie on planes $t = 10^4$ and $t = 10^5$ s, respectively. The values of the parameters of the system are taken from [19, 28].

Therefore, the next step is to develop a solution that describes the process more accurately and takes into account some nonlinearities.

3.1. Analytical solution with non-linear liquidus surface equations and cotectic curve (similar temperature profile)

We consider the same process as in the previous section, but with some modifications—the liquidus surface equations will be investigated in a general form that does not imply linearity in impurity concentrations.

The phase transition temperature T_*^p in the main two-phase zone depends on the concentrations of the components B and C and has the following form:

$$T = T_*^p = F(B, C). \tag{68}$$

In a cotectic two-phase zone, temperature and impurity concentrations can be written as:

$$T = T_*^c = F_1^c(B) = F_2^c(C). \tag{69}$$

In the case of linearity of the liquidus surface, we have:

$$\begin{aligned} T_*^p &= T_* + m_B B + m_C C, \\ T_*^c &= -m_B^c(B - B_E) + T_E = -m_C^c C + T_E^{AB}. \end{aligned} \tag{70}$$

In addition, we use the linearity of the temperature profile in the two-phase zones and solids:

$$T_p(z,t) = T_1(t) + T_2(t) z. \tag{71}$$

As noted earlier, the concentration field in the main two-phase zone instead of (16) and (17) will be described by the Scheil equations [40, 41]:

$$\frac{\partial}{\partial t}\left((1-\varphi_A)B_p\right) = 0, \quad \frac{\partial}{\partial t}\left((1-\varphi_A)C_p\right) = 0. \tag{72}$$

The equations are good approximations for many experiments (see, e.g. [29, 31]), because in such situations impurity transport is almost independent of diffusion flux and mainly depends on its displacement by the growing solid phase.

Integration of equations (72) defines the concentration distributions in the main two-phase zone as implicit functions of spatial coordinate and time (instead of 43):

$$B_p(z,t) = \frac{B_{pb}}{1-\varphi_A}, \quad C_p(z,t) = \frac{C_{pb}}{1-\varphi_A}. \tag{73}$$

At any point of the considered two-phase zone $C/B = C_{pb}/B_{pb}$ (constants B_{pb} and C_{pb} represent values of B and C at the boundary $z = h_p(t)$, where $\varphi_A = 0$).

Substituting the distributions (71) and (73) into the equation (68) defining the liquidus surface we determine the solid phase fraction distribution φ_A, which can be easily expressed as an inverse function $z = z(\varphi_A, t)$:

$$T_1 + T_2 z = F\left(\frac{B_{pb}}{1-\varphi_A}, \frac{C_{pb}}{1-\varphi_A}\right) \equiv G(\varphi_A). \tag{74}$$

Note that the dependence on the constants B_{pb} and C_{pb} is omitted here.

The boundary conditions at $z = h_p(t)$ are written as (see (44)):

$$(B_{pb} - B_\infty)\frac{dh_p}{dt} = -D_B\frac{\partial B_p}{\partial z}, \quad (C_{pb} - C_\infty)\frac{dh_p}{dt} = -D_C\frac{\partial C_p}{\partial z}, \tag{75}$$

where B_∞ and C_∞ represent the values of B and C in the liquid phase away from the boundary h_p, and D_B and D_C are the diffusivity of substances B and C, respectively.

Further we obtain the relation between the boundary concentration values as:

$$C_{pb} = \frac{DB_{pb}C_\infty}{B_{pb}(D-1) + B_\infty}, \quad D = \frac{D_B}{D_C}. \tag{76}$$

The expression (76) is simplified and has the form of the ratio B/C already obtained above in the case of coincident diffusion coefficients ($C_{pb}/B_{pb} = C_\infty/B_\infty$).

Considering that:

$$\frac{\partial B_p}{\partial z} = \frac{B_{pb}}{(1-\varphi_A)^2}\frac{\partial \varphi_A}{\partial z}, \quad \frac{\partial C_p}{\partial z} = \frac{C_{pb}}{(1-\varphi_A)^2}\frac{\partial \varphi_A}{\partial z}, \tag{77}$$

we find the relationship between the temperature gradient and the velocity of the main two-phase liquid boundary from expressions (74) and (75) in a form:

$$T_2(t) = \frac{B_\infty - B_{pb}}{D_B B_{pb}}\left(\frac{dG}{d\varphi_A}\right)_{\varphi_A = 0}\frac{dh_p}{dt}. \tag{78}$$

As before, the solution of the heat equation in the liquid at $z > h_p(t)$ will be given as:

$$T_\ell(z,t) = T_\infty + (T_{pb} - T_\infty)\frac{\operatorname{erfc}\left(z/\sqrt{4\kappa_\ell t}\right)}{\operatorname{erfc}\left(h_p/\sqrt{4\kappa_\ell t}\right)}, \tag{79}$$

where κ_ℓ is the thermal diffusivity coefficient of the fluid.

Equating now the temperature gradients defined by the distributions (71) and (79) at $z = h_p(t)$, we obtain the relation between B_{pb} and h_p (noting that $T_{pb} = G(0)$):

$$\frac{(T_\infty - G(0))D_B B_{pb}}{\sqrt{\pi\kappa_\ell t}} = \operatorname{erfc}\left(\frac{h_p}{\sqrt{4\kappa_\ell t}}\right)\exp\left(\frac{h_p^2}{4\kappa_\ell t}\right)\left(\frac{dG}{d\varphi_A}\right)_{\varphi_A=0}\frac{dh_p}{dt}, \quad (80)$$

which is a generalised expression (49). Parameters $G(0)$ and $dG/d\varphi_A$ at $\varphi_A = 0$ depend only on the boundary value of the impurity concentration B_{pb} according to expressions (74) and (76).

The mass transfer equations (27) and (28) in the two-phase cotectic zone $h_c(t) < z < h_p(t)$ are also written in Scheil form:

$$\frac{\partial}{\partial t}(\chi B_c) + \frac{\partial \varphi_B}{\partial t} = 0, \quad \frac{\partial}{\partial t}(\chi C_c) = 0, \quad (81)$$

where the liquid phase fraction is $\chi(z,t) = 1 - \varphi_A(z,t) - \varphi_B(z,t)$. Integration of equations (81) gives the concentration distributions in the cotectic zone:

$$B_c(z,t) = \frac{B_{cb}(1 - \varphi_{AC}^- - \varphi_{BC}^-) + \varphi_{BC}^- - \varphi_B}{1 - \varphi_A - \varphi_B}, \quad (82)$$

$$C_c(z,t) = \frac{C_{cb}(1 - \varphi_{AC}^- - \varphi_{BC}^-)}{1 - \varphi_A - \varphi_B}, \quad (83)$$

where B_{cb} and C_{cb} are the values of B and C on the boundary $z = h_c$, and φ_{AC}^- and φ_{BC}^- are the fraction values of φ_A and φ_B computed on the left side of this boundary, respectively.

By equating the concentration ratios at the boundary $z = h_p$ and taking into account the expression (76), we obtain the boundary value C_{cb} that depends only on B_{cb} and B_{pb}:

$$C_{cb} = \frac{DB_{cb}C_\infty}{B_{pb}(D-1) + B_\infty}. \quad (84)$$

As in previous section, we assume that the temperature field in the cotectic zone is described by the distribution (74) with constant coefficients T_1 and T_2. Equating (68) and (74) at $z = h_c(t)$, we have:

$$F(B_{cb}, C_{cb}) \equiv f(B_{cb}, B_{pb}) = T_1 + T_2 h_c(t).$$

Assuming that $T_1 = T_{pb} - T_2 h_p(t) = G(0) - T_2 h_p(t)$ (this follows from the substitution (74) at the boundary point $z = h_p$), we determine the interface coordinate of the two phase zones as:

$$h_c(t) = h_p(t) + \frac{f(B_{cb}, B_{pb}) - G(0)}{T_2(t)}. \quad (85)$$

Equating the temperature to the cotectic temperature (69) at the boundary $z = h_c(t)$, we obtain two equations:

$$f(B_{cb}, B_{pb}) = T_1^c(B_{cb}), \quad f(B_{cb}, B_{pb}) = T_2^c(C_{cb}) = T_2^c(B_{cb}, B_{pb}). \quad (86)$$

The first of these equations defines the dependence $B_{cb} = B_{cb}(B_{pb})$, and the second one determines the function T_2^c.

Substituting $z = h_c(t)$ into the temperature distribution in the main two-phase zone and considering expression (85), we find the equation defining the boundary value of the solid phase fraction $\varphi_A = \varphi_{AC}^+$ to the right of the interface between the two-phase zones:

$$f(B_{cb}, B_{pb}) \equiv f_1(B_{pb}) = G(\varphi_{AC}^+). \quad (87)$$

Note that φ_{AC}^+ depends only on the boundary value B_{pb}.

The distributions of the fractions φ_A and φ_B in the cotectic zone can be easily found as inverse functions from the equality of expressions (69) and (71) at all points of this region:

$$T_1 + zT_2 = F_1^c(\varphi_A, \varphi_B), \quad T_1 + zT_2 = F_2^c(\varphi_A, \varphi_B), \quad (88)$$

where the expressions (82) and (83) are taken into account.

The temperature field in the solid phase at $0 < z < h_e(t)$ is represented by (71):

$$T_s(z,t) = T_1 + T_2 z = T_B + \frac{T_E - T_B}{h_e(t)}z, \quad T_1 + h_e T_2 = T_E,$$

where

$$h_e(t) = \frac{T_E - T_1}{T_2} = h_p(t) + \frac{T_E - G(0)}{T_2}. \quad (89)$$

Taking the equality $T_E - T_B = T_2 h_e$ into account, we obtain the moving coordinate of the boundary solid phase—cotectic zone:

$$h_e(t) = \frac{T_E - T_B}{G(0) - T_B}h_p(t). \quad (90)$$

By equating the expressions (89) and (90) and considering the temperature gradient (78), we obtain a differential equation for the boundary $h_p(t)$. Integrating this equation, we have:

$$h_p(t) = \sqrt{\beta_p^2 t + h_p(0)}, \quad \beta_p = \sqrt{\frac{2(G(0) - T_B)D_B B_{pb}}{(B_\infty - B_{pb})(dG/d\varphi_A)_{\varphi_A=0}}}. \quad (91)$$

Considering now that at the initial time $h_p = 0$, from (85), (90) and (91) we express the coordinates of the moving boundaries as:

$$h_e(t) = \beta_e\sqrt{t}, \quad h_c(t) = \beta_c\sqrt{t}, \quad h_p(t) = \beta_p\sqrt{t}, \quad (92)$$

where

$$\beta_e = \beta_p\frac{T_E - T_B}{G(0) - T_B}, \quad \beta_c = \beta_p + \frac{2(f(B_{cb}, B_{pb}) - G(0))D_B B_{pb}}{(B_\infty - B_{pb})\beta_p(dG/d\varphi_A)_{\varphi_A=0}}.$$

Expressions (92), as in the case of linearity of the liquidus surface, show the proportionality to the square root of time.

Combining now the expressions (80) and (92), we obtain a transcendental equation for the constant B_{pb}. After a minor transformation, we have:

$$\frac{2(T_\infty - G(0))D_B B_{pb}}{(B_\infty - B_{pb})\sqrt{\pi\kappa_\ell}\beta_p} = \operatorname{erfc}\left(\frac{\beta_p}{\sqrt{4\kappa_\ell}}\right)\exp\left(\frac{\beta_p^2}{4\kappa_\ell}\right)\left(\frac{dG}{d\varphi_A}\right)_{\varphi_A=0}. \tag{93}$$

The boundary values φ_{AC}^- and φ_{BC}^- are determined from the boundary conditions at $z = h_c(t)$ from expressions (21) and (22). Calculating now the derivatives in the right-hand sides of these equations using the expressions (74), (77) and (69), (71), given the relations (78) and (92), we find boundary values for the solid phase fraction as:

$$\varphi_{AC}^- = x - \varphi_{BC}^-,\quad \varphi_{BC}^- = \frac{1}{x_1}\left(B_{pb}x_2 - \frac{1-x}{(dF_1^c/dB)_{B_{cb}}} - B_{cb}(\varphi_{AC}^+ - x)x_1\right), \tag{94}$$

where

$$x = \frac{1 + (DC_{cb}x_1\varphi_{AC}^+ - C_{pb}x_2)(dF_2^c/dC)_{C_{cb}}}{1 + DC_{cb}x_1(dF_2^c/dC)_{C_{cb}}},$$

$$x_1 = \frac{\beta_c B_{pb}}{\beta_p(B_\infty - B_{pb})(dG/d\varphi_A)_{\varphi_A=0}},\quad x_2 = (1-\varphi_{AC}^+)^{-1}\left(\frac{dG}{d\varphi_A}\right)_{\varphi_{AC}^+}^{-1},$$

and the lower indices at the derivatives indicate their calculation points.

The boundary values of the fractions φ_{AE}^+ and φ_{BE}^+ to the right of the solid phase-cotectic zone boundary are defined by equations (88) at $z = h_e(t)$, and the boundary values of the fractions φ_{BE}^- and φ_{CE}^- ($\varphi_{AE}^- = 1 - \varphi_{BE}^- - \varphi_{CE}^-$) to the left of this boundary can be found from the mass balance boundary conditions (32) and (33). Calculating the gradients in the right-hand sides of these expressions using the relations (69), (71), and considering the expressions (78) and (92), we arrive at the result as:

$$\varphi_{BE}^- = \varphi_{BE}^+ + (1 - \varphi_{AE}^+ - \varphi_{BE}^+)\left[B_E + \frac{q}{(dT_1^c/dB)_{B_E}}\right], \tag{95}$$

$$\varphi_{CE}^- = (1 - \varphi_{AE}^+ - \varphi_{BE}^+)\left[C_E + \frac{q}{D(dT_2^c/dC)_{C_E}}\right], \tag{96}$$

where

$$q = \frac{(B_\infty - B_{pb})\beta_p}{B_{pb}\beta_e}\left(\frac{dG}{d\varphi_A}\right)_{\varphi_A=0}.$$

Thus, the solution of the problem describing the solidification of three-component systems in the presence of two moving phase transition regions for the liquidus surface in the general case, is completely defined by expressions (68), (69), (71), (73), (76), (78), (79), (82)–(84), (86)–(88) and (91)–(96). We note specifically that the linear temperature profile in the solid phase and two-phase zones, as already mentioned, is quite often observed in laboratory and field observations, and has a simple physical explanation. The second theoretical simplification, using the Scheil equations, demonstrates that actually, it does not affect the obtained results because the dominant factor is the displacement of impurity by the growing solid phase.

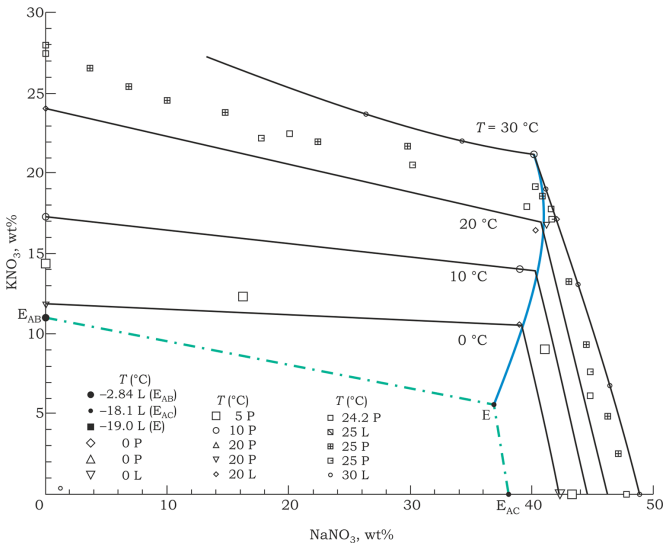

Figure 11. Phase diagram [19] of the crystallization process for the system H_2O-KNO_3-$NaNO_3$ in orthogonal coordinates. The data are taken from [42] and [43]. The thin dotted and solid lines are approximate cotectic curves based on the available data.

As noted above, linear liquidus functions (70) do not always satisfactorily describe experimental data (see figure 11). For many processes in metallurgy and geophysics, there are deviations from such linear relationships (see, for example, [19, 44, 45]). The simplest way to solve the problem is to approximate these deviations by quadratic liquidus equations. Thus, for example, for the ternary systems, the following dependencies can be used instead of the equation (70):

$$T_*^p = F(B,C) = T_* + m_B B + m_C C + n_B B^2 + n_C C^2 + n_{BC}BC = G(\varphi_A), \tag{97}$$

$$T_*^c = F_1^c(B) = -m_B^c(B - B_E) + T_E + n_B^c(B - B_E)^2, \tag{98}$$

$$T_*^c = F_2^c(C) = -m_C^c C + T_E^{AB} + n_C^c C^2, \tag{99}$$

where n_B, n_C, n_{BC}, n_B^c and n_C^c are the quadratic coefficients of the liquidus surface (in (97) the relations (73) are considered). In this situation, the solid phase fraction distributions $\varphi_A(z,t)$ and $\varphi_B(z,t)$ in the main and cotectic two-phase zones are solutions of the square equations obtained by substituting the explicit dependencies $G(\varphi_A)$, $F_1^c(B)$ and $F_2^c(C)$ into equations (74) and (88), while the boundary value φ_{AC}^+ is determined from quadratic equation (87). To define the three coefficients included in the expressions (97)–(99), as in the linear case, we have three points—the melting point, the eutectic point of the binary system and the eutectic point of the ternary system. The remaining coefficients should be determined from additional measurements.

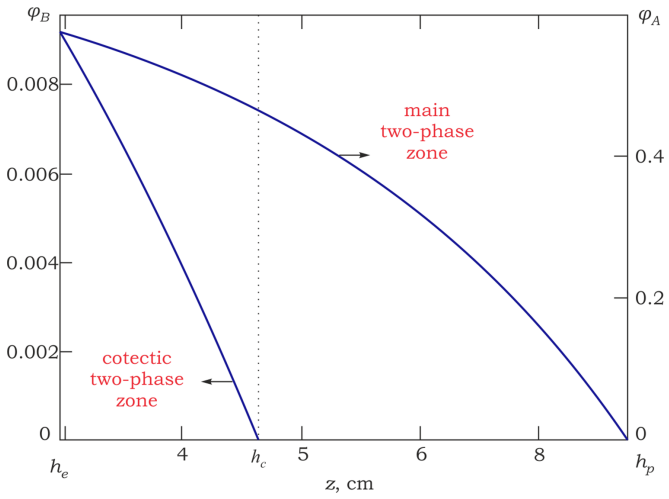

Figure 12. Distribution of the solid phase fraction in the two-phase zones at time $t = 10^5$ s. The vertical line shows the position of the interface between the two phase zones. Areas I and II represent the cotectic and main two-phase zones, respectively.

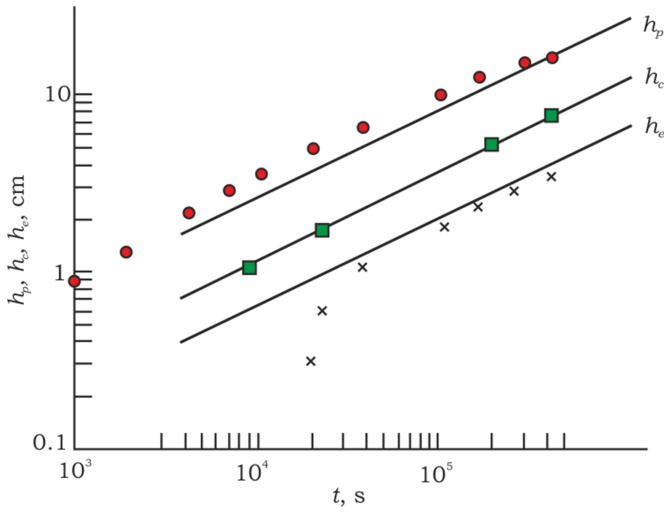

Figure 13. Interfacial boundary coordinates vs. time (the symbols show experimental data [19]).

Figures 12 and 13 show solid phase distributions and interface dynamics for a $H_2O - KNO_3 - NaNO_3$ salt solution which thermal properties are given in table 1. We also used the same solution in the previous section as the considering substance (with $C_\infty = 15.2$wt% $NaNO_3$ and $B_\infty = 3.5$wt% KNO_3). Calculations account for the deviation from the linear phase diagram by using the principal term of small order in the relation (97) proportional to C^2 (parameters $n_B = 0$, $n_{BC} = 0$, $n_B^c = 0$, $n_C^c = 0$, and $n_C = -6.8 \times 10^{-3}$ °Cwt%^{2} was determined from the experimentally known phase transition temperature $T_{pb} = -6.3$ °C at the boundary $z = h_p(t)$ [19]).

Figure 13 illustrates the movement of interphase boundaries according to expressions (92), and one can see that almost half of the entire phase transition region is a cotectic two-phase zone even with a small amount of component B in the system. During the solidification of multicomponent solutions and melts, the entire phase transition region consists of several phase transition regions of their components. In this case, as expressions (91) and (92) show, the external boundaries $h_p(t)$ and $h_e(t)$ of the total phase transition region do not depend on the parameters of the cotectic zone, but are determined only by the system operating parameters (T_B, T_∞, B_∞, C_∞) and the type of phase diagram. This means that the laws of motion of the external boundaries defined by expressions (92) will be valid for multicomponent systems. Note also that the addition of impurity in the system leads to a decrease in the phase transition temperature $G(0)$ at the two-phase zone-liquid boundary and, according to expressions (91) and (92), to a slower motion of both boundaries of the entire phase transition region.

3.2. *Analytical solution with non-linear liquidus surface equations and cotectic curve (different temperature profiles)*

The experiment shows (see e.g. figure 5) that the temperature profiles in the zones are slightly different from each other, although they have an almost linear form. To take into account this more general case, we carry out another study extending the results already obtained and allowing us to make more accurate calculations for the solidification process of multicomponent systems.

We will assume that the crystallization process has self-similar properties (see (55), (65) and (66) or (92)), so we represent the boundary positions and the self-similar variable η in the form:

$$h_e(t) = 2\lambda_e\sqrt{\kappa_\ell t},\quad h_c(t) = 2\lambda_c\sqrt{\kappa_\ell t},\quad h_p(t) = 2\lambda_p\sqrt{\kappa_\ell t}, \tag{100}$$

$$\eta = \frac{z}{2\sqrt{\kappa_\ell t}}. \tag{101}$$

Here λ_e, λ_c, and λ_p are the parabolic growth rate constants to be determined as the problem solution.

We suggest that the temperature fields are linear in η. In addition, we use the equations for the concentration fields in the Scheil form ((73) and (81)). Then the temperature and concentrations will be obtained explicitly:

$$T_p(\eta) = T_1 + \eta T_2 = F(B, C), \tag{102}$$

$$B_p(\eta) = \frac{B_{pb}}{1 - \varphi_A(\eta)},\quad C_p(\eta) = \frac{C_{pb}}{1 - \varphi_A(\eta)}, \tag{103}$$

in the main two-phase zone $\lambda_c < \eta < \lambda_p$, and:

$$T_c(\eta) = T_3 + \eta T_4 = F_1^c(B) = F_2^c(C), \tag{104}$$

$$B_c(\eta) = \frac{B_{cb}(1 - \varphi_{AC}^- - \varphi_{BC}^-) + \varphi_{BC}^- - \varphi_B(\eta)}{1 - \varphi_A(\eta) - \varphi_B(\eta)}, \tag{105}$$

$$C_c(\eta) = \frac{C_{cb}(1 - \varphi_{AC}^- - \varphi_{BC}^-)}{1 - \varphi_A(\eta) - \varphi_B(\eta)}, \tag{106}$$

in the cotectic two-phase zone $\lambda_e < \eta < \lambda_c$, and in the solid phase:

$$T_s(\eta) = T_B + \frac{T_E - T_B}{\lambda_e}\eta. \tag{107}$$

The boundary conditions (8)–(11) in self-similar variables are:

$$T_\ell = T_p = T_{pb} = F(B_{pb}, C_{pb}), \tag{108}$$

$$\frac{dT_\ell}{d\eta} = \frac{dT_p}{d\eta}, \quad \varphi_A = 0, \tag{109}$$

$$2\kappa_\ell\lambda_p(B_{pb} - B_\infty) = -D_B\frac{dB}{d\eta}, \quad 2\kappa_\ell\lambda_p(C_{pb} - C_\infty) = -D_C\frac{dC}{d\eta}, \tag{110}$$

and we have considered the most common case where $\varphi_A = 0$ with $\eta = \lambda_p$.

Combining the expressions (102) and (108), we find T_1 and T_{pb}:

$$T_1 = F(B_{pb}, C_{pb}) - \lambda_p T_2, \quad T_{pb} = F(B_{pb}, C_{pb}). \tag{111}$$

The derivatives of the concentrations with respect to the self-similar variable η are:

$$\frac{dB_p}{d\eta} = \frac{B_{pb}}{(1-\varphi_A)^2}\frac{d\varphi_A}{d\eta}, \quad \frac{dC_p}{d\eta} = \frac{C_{pb}}{(1-\varphi_A)^2}\frac{d\varphi_A}{d\eta}. \tag{112}$$

Substituting this into the boundary conditions (110), we express C_{pb} through B_{pb}:

$$C_{pb} = \frac{DB_{pb}C_\infty}{B_{pb}(D-1) + B_\infty}, \quad D = \frac{D_B}{D_C}. \tag{113}$$

Equations (102) and (103) determine implicitly the solid phase fraction $\varphi_A(\eta)$ in the main two-phase zone:

$$T_1 + \eta T_2 = F\left(\frac{B_{pb}}{1-\varphi_A}, \frac{C_{pb}}{1-\varphi_A}\right) \equiv G(\varphi_A), \tag{114}$$

and

$$\frac{d\varphi_A}{d\eta} = T_2\left(\frac{dG}{d\varphi_A}\right)^{-1}.$$

Substituting (112) into (110) at $\varphi_A = 0$, we arrive at the expression for T_2:

$$T_2 = \frac{2\kappa_\ell\lambda_p(B_\infty - B_{pb})}{D_B B_{pb}}\left(\frac{dG}{d\varphi_A}\right)_{\varphi_A=0}. \tag{115}$$

We obtain the relation between the unknown parameters B_{pb} and λ_p from (79), (102), (109) and (115) as:

$$\frac{(T_\infty - G(0))D_B B_{pb}}{\sqrt{\pi}\kappa_\ell} = \lambda_p(B_\infty - B_{pb})\mathrm{erfc}(\lambda_p)\exp(\lambda_p^2)\left(\frac{dG}{d\varphi_A}\right)_{\varphi_A=0}. \tag{116}$$

$$\lambda_c = \lambda_p + \frac{1}{T_2}\left[F\left(\frac{B_{pb}}{1-\varphi_{AC}^+}, \frac{C_{pb}}{1-\varphi_{AC}^+}\right) - G(0)\right]. \tag{117}$$

At the boundary between the zones $\eta = \lambda_c$, we have:

$$T_p = T_c, \quad \frac{B_{pb}}{1-\varphi_{AC}^+} = B_{cb}, \quad \frac{C_{pb}}{1-\varphi_{AC}^+} = C_{cb}, \quad \varphi_{BC}^+ = 0. \tag{118}$$

Substituting (102) and (104) into (118), we get explicit expressions for T_3, C_{cb} and φ_{AC}^+:

$$T_3 = T_1 + \lambda_c(T_2 - T_4), \quad C_{cb} = B_{cb}\frac{C_{pb}}{B_{pb}}, \quad \varphi_{AC}^+ = 1 - \frac{B_{pb}}{B_{cb}}. \tag{119}$$

In addition, the ratios (102) and (104) at $\eta = \lambda_c$ allow us to find the equation for $B_{cb} = B_{cb}(B_{pb})$:

$$F\left(B_{cb}, \frac{C_{pb}}{B_{pb}}B_{cb}\right) = F_1^c(B_{cb}). \tag{120}$$

Now, from this equation, we can conclude that λ_c defined by the expression (117) depends only on B_{pb} and λ_p.

The boundary conditions (20)–(22) at $\eta = \lambda_c$ in self-similar variables are:

$$2\lambda_c\kappa_\ell\rho_s L\left(\varphi_{AC}^+ - \varphi_{AC}^- - \varphi_{BC}^-\right) = \left[(1-\varphi_{AC}^+)k_\ell + \varphi_{AC}^+ k_s\right]T_2 - \left[(1-\varphi_{AC}^- - \varphi_{BC}^-)k_\ell + (\varphi_{AC}^- + \varphi_{BC}^-)k_s\right]T_4, \tag{121}$$

$$\frac{2\lambda_c\kappa_\ell}{D_B}\left(B_{cb}(\varphi_{AC}^+ - \varphi_{AC}^-) + (1-B_{cb})\varphi_{BC}^-\right) = B_{cb}T_2\left(\frac{dG}{d\varphi_A}\right)_{\varphi_{AC}^+}^{-1} - \left(1-\varphi_{AC}^- - \varphi_{BC}^-\right)T_4\left(\frac{dF_1^c}{dB_c}\right)_{B_{cb}}^{-1}, \tag{122}$$

$$\frac{2\lambda_c\kappa_\ell}{D_C}C_{cb}\left(\varphi_{AC}^+ - \varphi_{AC}^- - \varphi_{BC}^-\right) = C_{cb}T_2\left(\frac{dG}{d\varphi_A}\right)_{\varphi_{AC}^+}^{-1} - \left(1-\varphi_{AC}^- - \varphi_{BC}^-\right)T_4\left(\frac{dF_2^c}{dC_c}\right)_{C_{cb}}^{-1}, \tag{123}$$

where

$$\frac{dB_c}{d\eta} = T_4\left(\frac{dF_1^c}{dB_c}\right)^{-1}, \quad \frac{dC_c}{d\eta} = T_4\left(\frac{dF_2^c}{dC_c}\right)^{-1}.$$

It is now easy to express φ_{AC}^-, φ_{BC}^- and T_4 from equations (121)–(123). The solid phase fractions $\varphi_A(\eta)$ and $\varphi_B(\eta)$ in the cotectic zone can be found from equations (104)–(106). Moreover, by equating the temperature distribution at $\eta = \lambda_e$ to the known temperature at the eutectic point of the ternary system E, we obtain three equations to determine φ_{AE}^+, φ_{BE}^+ and λ_e. For example, for λ_e we have:

$$\lambda_e = \frac{T_E - T_3}{T_4}. \tag{124}$$

The solid phase fractions φ^-_{AE}, φ^-_{BE} and φ^-_{CE} left of solid phase boundaries $\eta = \lambda_e$ can be found as before from the boundary conditions (32) and (33):

$$\varphi^-_{BE} = \frac{D_B}{2\lambda_e\kappa_\ell}\left(1-\varphi^+_{AE}-\varphi^+_{BE}\right)T_4\left(\frac{dF^c_1}{dB_c}\right)^{-1}_{B_E} - B_E\left(\varphi^+_{AE}+\varphi^+_{BE}-1\right)+\varphi^+_{BE},\quad \varphi^-_{AE} = 1-\varphi^-_{BE}-\varphi^-_{CE}, \tag{125}$$

$$\varphi^-_{CE} = \frac{D_C}{2\lambda_e\kappa_\ell}\left(1-\varphi^+_{AE}-\varphi^+_{BE}\right)T_4\left(\frac{dF^c_2}{dC_c}\right)^{-1}_{C_E} - C_E\left(\varphi^+_{AE}+\varphi^+_{BE}-1\right). \tag{126}$$

In order to obtain the second relation between B_{pb} and λ_p, we use the heat balance condition (31) at the solid phase/cotectic two-phase interface:

$$2\lambda_e\kappa_\ell\rho_s L\left(\varphi^+_{AE}+\varphi^+_{BE}-1\right) = T_4\left[\left(1-\varphi^+_{AE}-\varphi^+_{BE}\right)k_\ell+\left(\varphi^+_{AE}+\varphi^+_{BE}\right)k_s-\frac{T_E-T_B}{T_E-T_3}k_s\right]. \tag{127}$$

Thus, the two unknowns B_{pb} and λ_p can be found from equations (116) and (127), the remaining process parameters are determined from expressions (102)–(107), (111)–(115) and (121)–(126).

We use the quadratic dependences for the liquidus surface, as in the previous section, to obtain specific results:

$$T^p_* = T_M + m_B B + m_C C + n_C C^2,\quad h_c(t) < z < h_p(t),$$

$$T^c_* = -m^c_B(B-B_E)+T_E = -m^c_C C + n^c_C C^2 + T^{AB}_E \quad h_e(t) < z < h_c(t).$$

Remind that from the three points of the liquidus surface and the value $T_{pb} \approx -6.3$ °C we find the expansion coefficients:

$$m_B = \frac{T^{AB}_E - T_M}{B^{AB}_E},\quad m_C = \frac{T_E - T_M - m_B B_E - n_C C^2_E}{C_E},$$

$$m^c_B = \frac{T^{AB}_E - T_E}{B_E - B^{AB}_E},\quad m^c_C = \frac{T^{AB}_E - T_E + n^c_C C^2_E}{C_E},$$

$$n_C = \frac{1}{C_\infty(C_\infty - C_E)}\left(T_* - T_M - m_B B_\infty - (T_E - T_M - m_B B_E)\frac{C_\infty}{C_E}\right),$$

$$n^c_C = \frac{B^2_\infty}{B_{cb}C_\infty(B_{cb}C_\infty - C_E B_\infty)} \times\left(T_M + m_B B_{cb} + m_C B_{cb}\frac{C_\infty}{B_\infty} + n_C B^2_{cb}\frac{C^2_\infty}{B^2_\infty} + \frac{B_{cb}C_\infty}{C_E B_\infty}\left(T^{AB}_E - T_E\right) - T^{AB}_E\right).$$

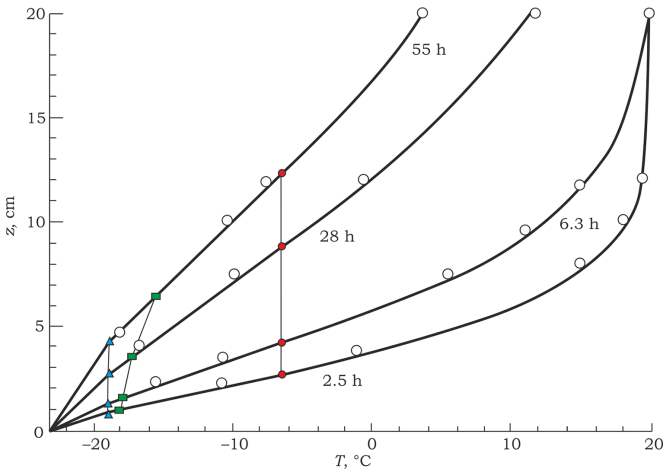

Figure 14. Temperature profiles for different time values (numbers at the curves). The circles show the experimental data (experiment 7, [19]). Icons on the curves are the positions of the main two-phase zone-liquid boundary (shaded circles), cotectic two-phase zone-main two-phase zone (shaded squares) and cotectic two-phase zone-liquid.

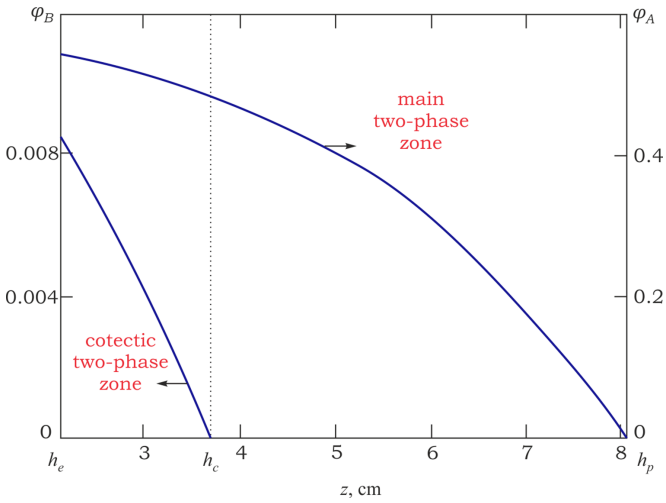

Figure 15. Distribution of the solid phase fraction in the two-phase zones at time $t = 10^5$ s. The vertical line shows the position of the interface between the two phase zones. Areas I and II respectively represent the cotectic and main two-phase zones.

Figures 14–16 show the obtained temperature, phase fraction and concentration distributions, respectively, for the system $H_2O - KNO_3 - NaNO_3$ whose thermophysical parameters are given in table 1. Figure 14 shows the temperature profiles in all solidification regions for different solidification times (similar to figure 7). Figure 15 is given to compare the distribution of phase fractions with similar data from more specific cases. Figure 16 shows distributions of impurity concentrations for various values of the initial concentration of component B. It can be seen that its variation does not strongly affect the pure solid-liquid boundaries (left and right boundaries of all curves), but it significantly changes the position of the boundary between the two two-phase zones.

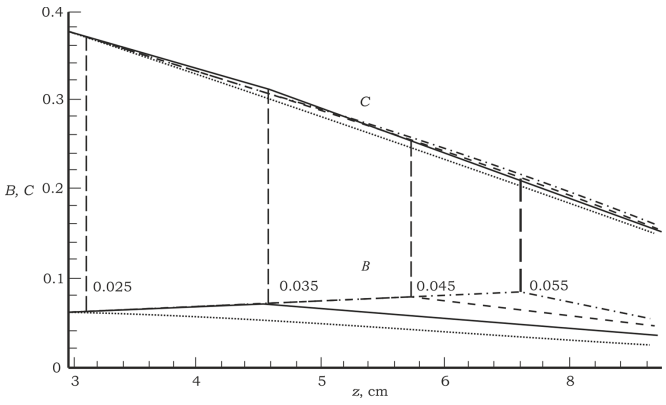

Figure 16. The concentrations of the components B and C in the zones at time $t = 10^5$ s. The vertical dashed lines mark the position of the boundary between the two two-phase zones at different values of B_∞ (numbers next to the lines), whereas the solid phase boundary $h_e \approx 2.94$ cm and the liquid phase $h_p \approx 8.7$ cm remain virtually unchanged at different B_∞.

We conclude the section by summarizing the results. The assumptions about the linearity of the liquidus surface and temperature were excluded from the model of directional solidification of three-component systems with two-phase zones, which allowed us to obtain a more mathematically rigorous and extensible method for solving such problems. The obtained analytical solution complements the already existing experimental data, numerical solutions, and less precise solutions of the second section. In addition, it has been shown that the theoretical approach described in this section can be used for multicomponent systems. In this case, the laws of motion for liquid phase/two-phase and solid phase/two-phase boundaries will be the same as for the three-component system; only the number of two-phase state zones will change. The results obtained in this section are in good agreement with experimental data and can be used for predicting the behavior and description of the crystallization process, including the distribution of impurities in the solidified samples.

4. Conclusion

In the present paper, the problem of three-component crystallization systems with two-phase zones—main and cotectic zones—was considered. The strong nonlinearity of the model in such processes makes it impossible to find an analytical solution in a general form. Several assumptions, consistent with the physical properties of the process and experimental data, were proposed in this paper. The liquidus surface was assumed to be linear and characterized the phase transition temperature dependence on the system components concentrations; moreover, the temperature linearity in the two-phase zones and the solid was assumed and their profiles were considered to coincide. As a result, an analytical solution of the equations of heat and mass transfer in the two-phase zones was obtained, making it possible to find distributions of temperature and concentrations of all components in all regions, shares of solid phases in both two-phase zones, velocities, and laws of motion of interphase boundaries. During the solution process, it was shown that the process is self-similar if the temperature at the liquid phase/main two-phase zone boundary is constant. Moreover, it was shown that the concentration of components that start to solidify in the cotectic two-phase zone has a weakly pronounced maximum at the interface of two-phase zones.

Let us especially note in conclusion that the theory of ternary melt crystallization with two two-phase layers in the steady-state manner (solidification velocity is constant) was detailed and discussed in [46]. The readers can find in this article a mathematical model of the steady-state solidification process with main and cotectic two-phase regions and a method for solving this non-linear solidification model with constant velocity. Note that exact analytical solutions of the non-linear model were derived in [46] in a parametric form. So, for example, it was shown that the crystallization velocity is entirely defined by temperature gradients in the solid and liquid layers. This growth law is identical to cases of binary melt crystallization with a two-phase layer. Also, it was shown that the liquid composition of the main dissolved impurity reduces in the cotectic and main regions, while the second (cotectic) impurity concentration increases in the cotectic region, attains a maximum value, and reduces in the main two-phase region. For more details of this quasi-stationary theory, we refer the interested reader to the theory [46].

The theory of directional crystallization of ternary melts with main and cotectic two-phase layers developed in this paper takes into account only the basic features of the solidification process. In future studies, this theory can be generalized to nonlinear heat and mass transfer in the two-phase region [34, 35, 47], the presence of melt flows [48–51], the morphological instability of the interfaces [51–54], stochastic temperature fluctuations, and the joint realization of bulk and directional solidification [55–58]. Such a generalization can be made by analogy with the theory developed in these works for the solidification of binary melts with a two-phase region. In addition, the analysis of the solid phase fraction distribution during solidification can be performed using CALPHAD [59, 60].

Data availability statement

No new data were created or analyzed in this study.

Acknowledgments

The present research work consists of theoretical, computational and experimental parts, which were supported by different financial sources. L V T gratefully acknowledges research funding from the Foundation for the Advancement of Theoretical Physics and Mathematics ‘BASIS’ (Project No. 21-1-3-11-1) for the theoretical part. Computational calculations and comparison with experiments were supported by the Ministry of Science and Higher Education of the Russian Federation (Project Number FEUZ-2020-0057). A A I, E V M and D V

A thank this foundation for the financial support of research studies.

ORCID iDs

L V Toropova https://orcid.org/0000-0003-4587-2630
D V Alexandrov https://orcid.org/0000-0002-6628-745X

References

[1] Herlach D, Galenko P and Holland-Moritz D 2007 *Metastable Solids From Undercooled Melts* (Amsterdam: Elsevier)
[2] Alexandrov D V and Alexandrova I V 2019 *Phil. Trans. R. Soc.* A **377** 20180209
[3] Kurz W, Fisher D J and Trivedi R 2019 *Int. Mater. Rev.* **64** 311
[4] Alexandrov D V and Galenko P K 2021 *Phil. Trans. R. Soc.* A **379** 20200325
[5] Alexandrov D V, Netreba A V and Malygin A P 2012 *Int. J. Heat Mass Trans.* **55** 1189
[6] Alexandrova I V, Alexandrov D V and Makoveeva E V 2021 *Phil. Trans. R. Soc.* A **379** 20200308
[7] Mullins W W and Sekerka R F 1964 *J. Appl. Phys.* **35** 444
[8] Borisov V T 1987 *Theory of Two-Phase Zone of Metallic Ingot* (Moscow: Metallurgia)
[9] Buyevich Y A, Alexandrov D V and Mansurov V V 2001 *Macrokinetics of Crystallization* (New York: Begell House Inc.)
[10] Alexandrova I V, Alexandrov D V, Aseev D L and Bulitcheva S V 2009 *Acta Phys. Pol.* A **115** 791
[11] Gradinger R 1996 *Mar. Ecol. Prog. Ser.* **131** 301
[12] Huppert H E and Sparks R S J 1980 *Contrib. Mineral. Petrol.* **75** 279
[13] Schneider M C and Beckermann C 1995 *Int. J. Heat Mass Transfer* **38** 3455
[14] Schneider M C, Gu J P, Beckermann C, Boettinger W J and Kattner U R 1997 *Metall. Mater. Trans.* A **28** 1517
[15] Gu J P, Beckermann C and Giamei A F 1997 *Metall. Mater. Trans.* **28** 1533
[16] Beckermann C, Gu J P and Boettinger W J 2000 *Metall. Mater. Trans.* **31** 2545
[17] Chen F, Lu J W and Yang T L 1994 *J. Fluid Mech.* **276** 163
[18] Aseev D L and Alexandrov D V 2006 *Acta Mater.* **54** 2401
[19] Aitta A, Huppert H E and Worster M G 2001 *J. Fluid Mech.* **432** 201
[20] West D R F 1982 *Ternary Equilibrium Diagrams* 2nd edn (London: Chapman and Hall)
[21] Smallman R E 1985 *Modern Physical Metallurgy* (Oxford: Butterworths)
[22] Boettinger W J, Kattner U R, Coriell S R, Chang Y A and Mueller B A 1995 *Modelling of Casting, Welding and Advanced Solidification Process VII* vol 649, ed M Cross and J Campbell (Warrendale, PA: SAE International)
[23] Krane M J M, Incropera F P and Gaskell D R 1997 *Int. J. Heat Mass Transfer* **40** 3827
[24] Krane M J M and Incropera F P 1997 *Int. J. Heat Mass Transfer* **40** 3837
[25] Krane M J M, Incropera F P and Gaskell D R 1998 *Metall. Mater. Trans.* A **29** 843
[26] Felicelli S D, Poirier D R and Heinrich J C 1997 *J. Cryst. Growth* **177** 145
[27] Felicelli S D, Poirier D R and Heinrich J C 1998 *Metall. Mater. Trans.* **29** 847
[28] Anderson D M J 2003 *J. Fluid Mech.* **483** 165
[29] Flemings M C 1974 *Solidification Processing* (New York: McGraw-Hill)
[30] Aitta A, Huppert H E and Worster M G 2001 Solidification in ternary systems *Interactive Dynamics of Convection and Solidification* vol 113, ed P Ehrhard, D S Riley and P H Steen (Dordrecht: Kluwer)
[31] Boettinger W J, Kattner U R and Banerjee D K 1998 *Modeling of Casting, Welding and Advanced Solidification Processes VIII* vol 159, ed B G Thomas and C Beckermann (Warredale, PA: SAE International)
[32] Martin S and Kauffman P 1974 *J. Fluid Mech.* **64** 507
[33] Worster M G 1986 *J. Fluid Mech.* **167** 481
[34] Alexandrov D V and Aseev D L 2005 *J. Fluid Mech.* **527** 57
[35] Alexandrov D V and Aseev D L 2006 *Comput. Mater. Sci.* **37** 1
[36] Huppert H E and Worster M G 1985 *Nature* **314** 703
[37] Wettlaufer J S, Worster M G and Huppert H E 2000 *J. Geophys. Res.* **105** 1123
[38] Kerr R C, Woods A W, Worster M G and Huppert H E 1990 *J. Fluid Mech.* **216** 323
[39] Kerr R C, Woods A W, Worster M G and Huppert H E 1990 *J. Fluid Mech.* **217** 331
[40] Scheil E 1942 *Z. Met.kd.* **34** 70
[41] Aseev D L and Alexandrov D V 2006 *Int. J. Heat Mass Transfer* **49** 4903
[42] Linke W F 1965 *Solubilities of Inorganic and Metal-Organic Compounds, Vol II* 4th edn (Washington, DC: American Chemical Society)
[43] Protsenko P I, Razumovskaya O N and Brykova N A 1971 *Guide to Solubility of Nitrite and Nitrate Salt Systems* ed A B Zhdanovsky (Leningrad: Chemistry)
[44] Hort M 1998 *J. Petrol.* **39** 1063
[45] Nizovtseva I G, Starodumov I O and Alexandrov D V 2020 *J. Phys.: Condens. Matter* **32** 304003
[46] Alexandrov D V and Malygin A P 2012 *Int. J. Heat Mass Transfer* **55** 3755
[47] Alexandrov D V, Yu D G, Malygin A P, Nizovtseva I G and Toropova L V 2017 *Russ. Metall.* **2017** 127
[48] Schulze T P and Worster M G 1998 *J. Fluid Mech.* **356** 199
[49] Solomon T H, Hartley R R and Lee A T 1999 *Phys. Rev.* E **60** 3063
[50] Chung C A and Worster M G 2002 *J. Fluid Mech.* **455** 387
[51] Toropova L V, Alexandrov D V, Rettenmayr M and Galenko P K 2020 *J. Cryst. Growth* **535** 125540
[52] Worster M G 1992 *J. Fluid Mech.* **237** 649
[53] Alexandrov D V and Ivanov A O 2000 *J. Cryst. Growth* **210** 797
[54] Mullins W W and Sekerka R F 1964 *J. Appl. Phys.* **35** 444
[55] Mansurov V V 1990 *Math. Comput. Model.* **14** 819
[56] Alexandrov D V, Ivanov A A and Alexandrova I V 2020 *J. Cryst. Growth* **532** 125420
[57] Alexandrov D V, Alexandrova I V, Ivanov A A, Malygin A P, Starodumov I O and Toropova L V 2019 *Russ. Metall.* **2019** 787
[58] Toropova L V and Alexandrov D V 2022 *Sci. Rep.* **12** 10997
[59] Zhang C, Miao J, Chen S, Zhang F and Luo A 2019 *J. Phase Equilib. Diffus.* **40** 495
[60] Xu K, Liu J, van der Zwaag S, Xu W and Li J 2022 *J. Mater. Sci. Technol.* **128** 98